- Technical Paper -

ALTERATION OF PORE STRUCTURE IN CEMENT PASTE UNDER DIFFERENT DRYING STATES BY NITROGEN SORPTION

Piyapong SUWANMANEECHOT[*1], Abudushalamu AILI[*2], Ippei MARUYAMA[*3]

ABSTRACT

Nitrogen sorption was measured for a study of the pore structure of low heat Portland cement paste (L-hcp) and high early strength Portland cement paste (H-hcp). The Grand Canonical Monte Carlo method (GCMC) simulated the pore size distribution under various RHs. When relative humidity started to decrease, gel pores gradually disappear. The loss of nitrogen surface area can be explained by C-S-H agglomeration. Based on GCMC, the large capillary pores presented the maximum volume at dried 40% RH. The L-hcp contained the higher porosity than the H-hcp based on the N_2 sorption measurements.

Keywords: calcium-silicate-hydrate (C-S-H), drying, nitrogen sorption, pore size distribution

1. INTRODUCTION

The desirable engineering properties of concrete are largely dependent on the characteristic of microstructure in cement paste. Particularly, main amorphous phase - calcium silicate hydrate (C-S-H) – in cement paste expresses colloidal nature [1, 2], which is affected by moisture state from surrounding environments. An inverse relationship between strength and porosity in C-S-H is crucial when C-S-H faces to varying temperatures and humidities.

To characterize the microstructural changes under different relative humidities, nitrogen sorption is often measured [3, 4]. One comprehensive assumption related to nitrogen sorption is that nitrogen molecules adsorb on the C-S-H surface but cannot access into interlayer spaces. BET nitrogen surface area therefore indicates the surface area of C-S-H excluding interlayer spaces [5]. Analysis of sorption isotherm with the Grand Canonical Monte Carlo method (GCMC) provides the insight into the pore size distribution.

In this study, low heat Portland cement, which is the representative of belite rich cement, and high early strength cement paste, which is represented as alite rich cement, are examined to compare the pore structure of hardened cement paste (hcp) under various relative humidities.

2. TEST PROGRAMS

2.1 Materials

(1) Cement

Two different types of cement were used to compare the pore structure between alite-rich and belite-rich cements. High early strength Portland cement (H) and low heat Portland cement (L) were examined by XRD/Rietveld analysis following the method in [6]. The mineral compositions of those are shown in Table 1.

Table 1 Mineral composition of cement H and L

Mineral	H	L
C_3S	65.56±2.20	20.11±1.60
C_2S	15.14±0.93	62.95±1.14
C_3A	6.75±0.29	1.95±0.43
C_4AF	7.96±0.47	10.71±0.60
Periclase	0.81±0.28	0.52±0.22
Bassanite	2.39±0.20	2.43±0.36
Gypsum	0.51±0.66	1.11±0.63
Total	99.12	99.78

(2) Experimental preparation

Hardened cement pastes of 0.55 w/c ratio were mixed with water, then moved to a controlled temperature room at 20 ± 1 °C for repeatedly remixing the fresh paste by using a spatula every 30 minutes for 6 hours until no segregation between paste and water. The paste was poured into molds, compacted on a vibration table, and kept in sealed conditions for 3 days. Before starting drying process, 3 × 13 × 100 mm specimens were cured in lime-saturated water for 1 year. The hydration almost fully completed during the one-year-curing cycle under lime-saturated water before drying [6].

The high early strength Portland specimens were dried in chambers in which the relative humidity was controlled by varying amount of sodium hydroxide in the solutions as shown in Table 2 [7]. Meanwhile, Table 3 [8] shows supersaturated salt solutions that were used to control relative humidity for the low heat Portland specimen in chambers. Drying period lasted for more than one year for both types of cement to ensure that microstructure is stable under different drying state. Moreover, the dried specimens were compared with wet specimens that is cured in lime-saturated water (100% relative humidity). Specimen code at a target relative humidity is named as H55_XXRH or L55_XXRH, where XX is the relative humidity.

*1 Doctoral student, Graduate School of Environmental Studies, Nagoya University, JCI Student Member
*2 Assistant professor, Graduate School of Environmental Studies, Nagoya University
*3 Professor, Graduate School of Environmental Studies, Nagoya University, JCI Member

Table 2 Concentration of sodium hydroxide

RH (%)	Concentration (%mass)	RH (%)	Concentration (%mass)
11	47.97	60	24.66
20	40.00	70	20.80
30	35.29	80	16.10
40	31.58	90	9.83
50	28.15	95	5.54

Table 3 Supersaturated salt solution

RH (%)	Salt	RH (%)	Salt
11	$LiCl_2$	79	NH_4Cl
33	$MgCl_2$	85	KCl
40	NaI	95	KNO_3
58	NaBr		

2.2 Method

The prismatic specimens dried at different relative humidities were pulverized (particles size 25 – 75 μm) for the nitrogen sorption analysis. Before the testing, a 100 ± 10 mg powder was dried using a vacuum pump for 4 hours at room temperature (20 °C). Pre-treatment at room temperature was applied instead at 105 °C to preserve original microstructure [9]. After the testing, dry mass of the powder was determined by heating at 105 °C to normalize the sorption isotherm. The nitrogen sorption isotherms were measured at 77.4 K by the volumetric method using BEL-sorpmini (MicrotracBEL). Taking the cross section of one nitrogen molecule equal to 0.162 nm^2 [5], the specific surface area was calculated using the Brunauer-Emmett-Teller (BET) theory [10] on adsorption branch between 0.05 and 0.35 relative pressure.

The Grand Canonical Monte Carlo (GCMC) is the famous computer simulation method for the study of fluid adsorption in pore structure of porous materials. This method was applied on the experimental data to simulate the pore size distribution.

3. RESULTS AND DISCUSSION

3.1 Sorption isotherms

The nitrogen sorption isotherms of the L55 and H55 samples dried under different relative humidities are summarized in Fig. 1. The x-axis of Fig. 1 was shifted to better compare the shape of isotherm. Based on IUPAC classification of adsorption isotherms [11], the shape of the sorption isotherms of samples dried at higher relative humidity (from L55_100%RH to L55_58%RH and H55_100%RH to H55_70%RH) are similar to characteristic feature of the type IV isotherm with its hysteresis loop by a sudden drop observed on desorption branch at relative pressure between 0.40 and 0.50. This type of isotherm indicates presence of small pores size and intermediate pores size in hcp. When the samples were further dried to 11% relative humidity, the shape of isotherms changed to the type V isotherm which do not present the small pores size in hcp and the cavitation-related sudden drop diminishes.

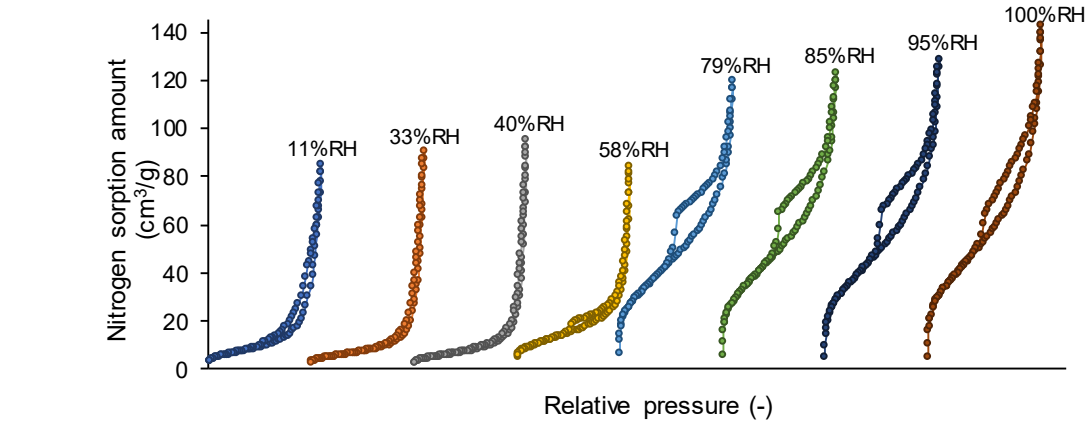

(a) L55

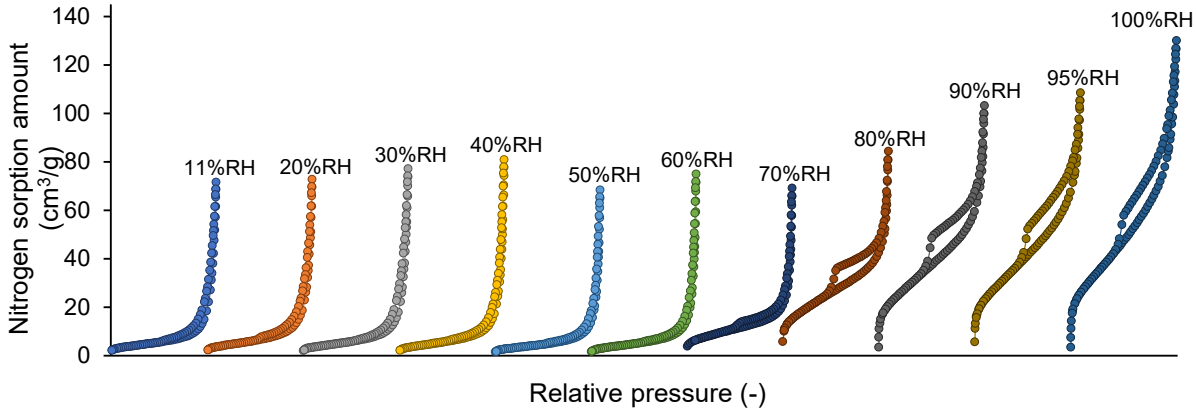

(b) H55

Fig. 1 The nitrogen sorption isotherms for L55 and H55 hcp samples dried at different relative humidities

Furthermore, for type IV isotherms, the amount of total sorption reduced continuously from the saturated condition to 58% relative humidity for L-hcp and to 70% relative humidity for H-hcp. When sorption isotherm changed from type IV to type V, total sorption amount increased, then decreased again until 11% relative humidity. Except with H-hcp dried at 50% and 60% relative humidity, total sorption was similar. For the same drying condition, L-hcp had a higher total sorption than H-hcp.

Fig. 2 presents the specific surface area of hcp as a function of the relative humidity. The nitrogen specific surface area decreased continuously from saturated condition to 40% and 60% relative humidity for L55 and H55, respectively. For samples dried lower than 40% relative humidity for L-hcp and 60% relative humidity for H-hcp, the nitrogen surface area remained constant. The large reduction in surface area appeared in samples dried at relative humidity range 40% to 90%. This result was similar to Parrott's results [3]. Furthermore, L-hcp had a higher surface area than H-hcp for the same drying relative humidity.

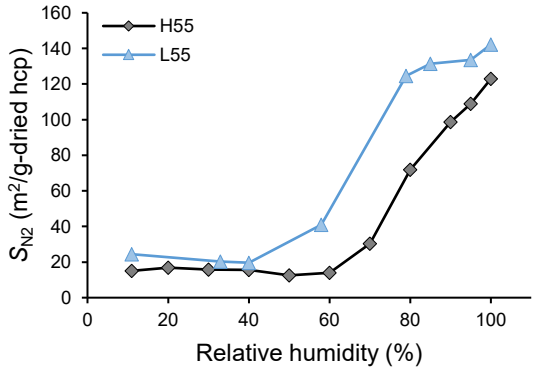

Fig. 2 Specific surface area of the hcp samples dried at different relative humidities

After drying for a long time, the loss of surface area illustrates that some capillary pores are closed [3] due to microstructural change of C-S-H under drying condition. The surface area remained constant because nitrogen cannot access to the pores created in the samples dried at relative humidity below 40% [12] and 60% for L-hcp and H-hcp, respectively.

3.2 The Grand Canonical Monte Carlo method (GCMC)

The Grand Canonical Monte Carlo method (GCMC) is a precise statistical simulation on the molecular level for the study of adsorption phenomena of fluids in pores [13]. This method simulates the adsorbed fluid condition in equilibrium by defining pore diameter and shape, placing the adsorptive molecules in the virtual space of pores, simulating the movement of adsorptive molecules based on thermodynamic criteria. Simulation of adsorption equilibrium gives the number of moles of molecules in the pores directly, and obtains the pore size distribution. In this process, GCMC requires a method to acquire an accurate equilibrium state by minimizing the difference between experiment and simulation.

GCMC was applied on the adsorption branch to obtain the pore size distribution by using BELMaster7 software (MicrotracBEL). According to IUPAC [11], N_2 sorption isotherms of hcp showed the shape of hysteresis loops similar to type H3 loop and type H4 loop, which are associated with slit-shaped pores and narrow slit-like pores, respectively. So, the pore model was assumed as a slit-shaped pore, and graphitic carbon structure was used as adsorbent. Although the potential energy of nitrogen adsorption on the graphite structure and the microstructure of C-S-H are different, but the relative relation will not be changed and give the same tendency. Tikhonov regularization was applied on simulation process to obtain the least deviation from the experimental data.

Many researches mentioned that N_2 is adsorbed only on the outside surface of C-S-H but does not access into interlayer space [4, 12]. Thus, the nitrogen sorption measurement can draw the picture of the alteration in mesoscale, which is outside C-S-H under different relative humidity. To consider alteration outside C-S-H, the pore size distribution is classified into two types; pore area distribution ($\mathrm{d}V_p/\mathrm{d}W$) and pore volume distribution ($\mathrm{d}V_p/\mathrm{dlog}W$). Pores with graphite structure were assumed to be slit shape with pore width (W). The pore area distribution is suitable for comparing the area of the reactive site (i.e. adsorbent) on the catalyst (i.e. adsorptive) during the reaction process. Meanwhile, the pore volume distribution is suitable for evaluation of adsorption capacity during the adsorption process especially on larger pores

Fig. 3 shows the pore area distribution of sample dried at different relative humidities. For the samples dried above 58% relative humidity, the GCMC results captured a population of the first peak (1.5 nm), the second peak (3.5 nm), and the third peak (10 nm). The high intensity of small pores of size (pore width < 5 nm) decreased with the decrease of relative humidity. This means that the small pores started to disappear from the samples dried at the preliminary state of drying. Moreover, the intensity of the pore width between 5 and 15 nm (i.e. intermediate pores of size) decreased simultaneously. For samples dried below 58% relative humidity, the first peak was at 10 nm and no distinct hump appeared at pore width smaller than 5 nm. The intensity of the first peak (10 nm) trended to increase with the decrease of relative humidity. Effect of strong drying induced the increase of intermediate pores and no appearance of small pores. For all relative humidities, the pore area distribution inclined from 15 nm to 100 nm and the difference for each drying condition cannot be observed. Furthermore, the peak intensity of L-hcp was higher than H-hcp.

It is noteworthy that the first peak (1.5 nm) and the second peak (3.5 nm) of samples dried above 58% relative humidity decreased with decreasing drying relative humidity in the same trend. The small pores under the first and the second peak region were lost significantly in the same proportion.

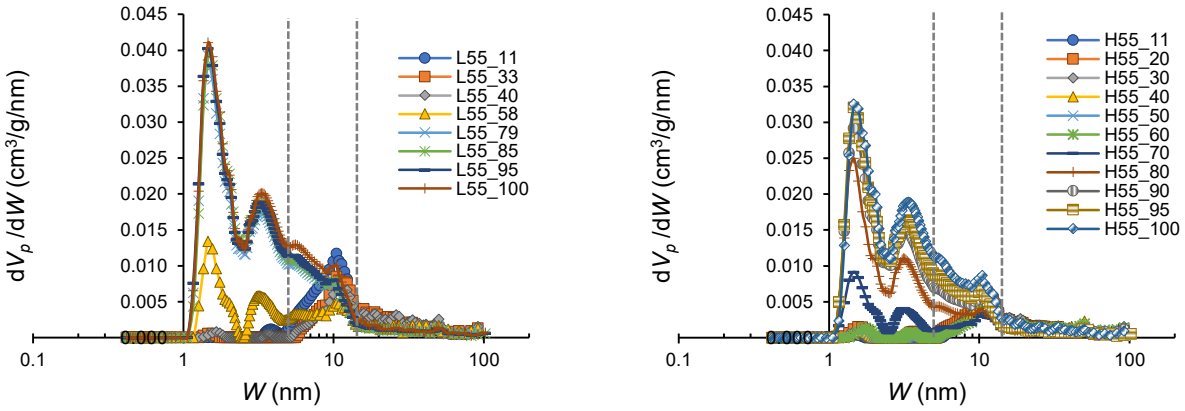

(a) L55 (b) H55

Fig. 3 Pore area distribution calculated by GCMC

When the intensity of the pore volume was plotted with pore width as shown in Fig. 4, different aspect can be observed particularly for large pores of size (pore width > 15 nm). The trend of pore volume distribution below 15 nm of pore width was similar to the pore area distribution. Surprisingly, the samples dried at 40% relative humidity clearly revealed a high intensity in the range 15-100 nm both L-hcp and H-hcp. There were two distinct peaks at 50 nm and 90 nm. For pore width larger than 15 nm, the pore volume of the samples dried at higher relative humidity was lower than the samples dried at lower relative humidity.

The change of pore size distribution by GCMC in hardened cement paste from saturated condition to drying condition reflected the alteration of C-S-H. The following evidences supports the above reason. Small pores in hcp at the beginning of drying state (above 58% relative humidity) gradually disappear due to capillary tensions. Meanwhile, for low relative humidities, no small pores were observed but the increase of intermediate pores (5-15 nm) were found (see clearly in Fig. 3 (a) and Fig. 4 (a)). If volume of small pores reduced, volume of large pores increased. For instant, the decrease of small pores in L55_58%RH (see Fig. 4 (a)) from saturated condition induced to the increase of the large pores from saturated condition.

3.3 Pore size classification

Based on the pore area distribution by GCMC, the pores in the hcp can be divided in three regions according to the distinct peaks: 1-5 nm; 5-15 nm; 15-100 nm. As mentioned previously, the first peak (1-2.5 nm) and the second peak (2.5-5 nm) of samples dried above 58% relative humidity changed proportionally in the same trend, so the region of those were merged into the pore width 1 to 5 nm for small pores. The pores that are detected by nitrogen sorption can be classified from the cumulative pore volume at given pore width. According to the previous literatures [1, 14], dV_{5-1} are defined as pore volume in the range of pore width between 1 and 5 nm as shown in Fig. 5 and reflect the gel pores in the hcp. Then, dV_{15-5} is defined as the increment of the cumulative pore volume from the pore width of 5 to 15 nm and is associated with the small capillary pores (i.e. interhydrate pores from ^{1}H NMR relaxometry method [15]). Finally, dV_{100-15} is defined as the difference of the cumulative pore volume between the pore width 15 and 100 nm and is related to the large capillary pores. Fig. 6 summarized the cumulative pore volume of the samples dried under different relative humidity both L-hcp and H-hcp.

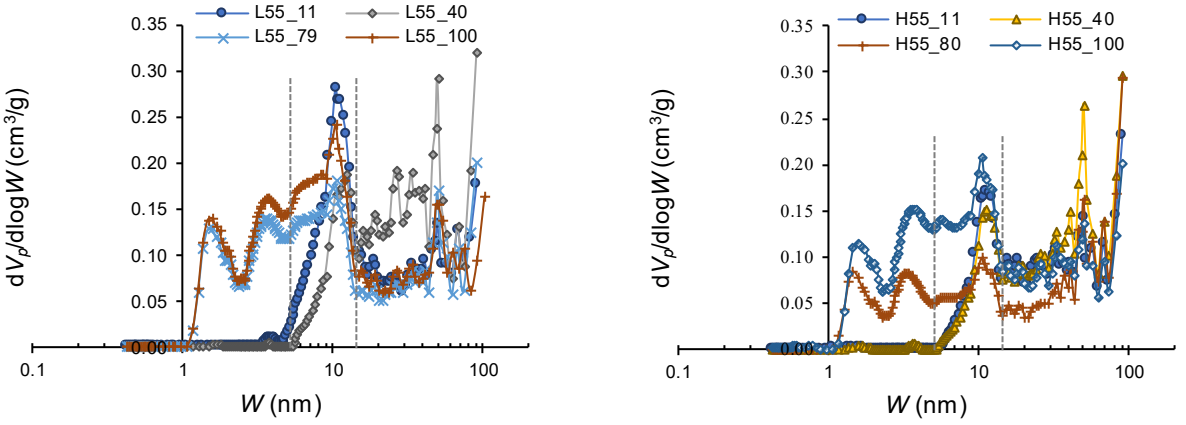

(a) L55 (b) H55

Fig. 4 Examples of pore volume distribution calculated by GCMC

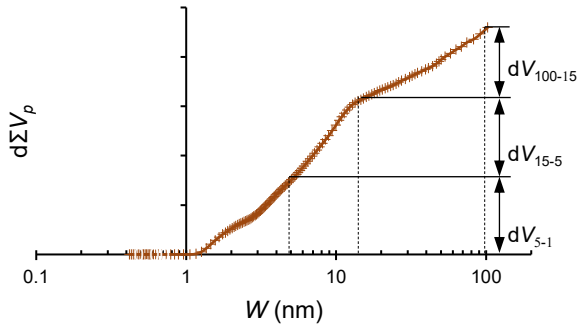

Fig. 5 Typical cumulative pore volume of hcp

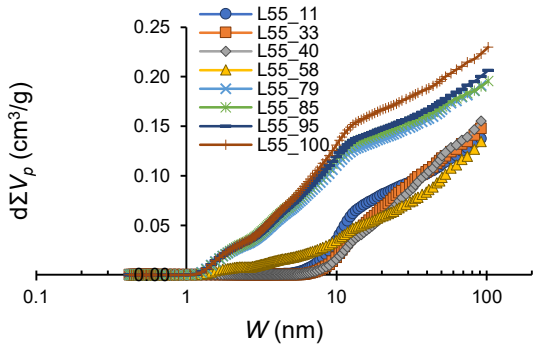

(a) L55

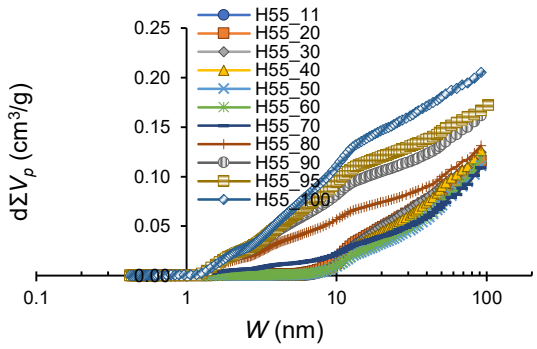

(b) H55

Fig. 6 Cumulative pore volume of the samples

The nitrogen sorption proportions of the samples dried at various relative humidities are shown in Fig. 7. For L55, the dV_{100-15} decreased from 100% to 85% relative humidity, increased from 85% to 40% relative humidity and then decreased from 40% to 11% relative humidity. As expected, H55 shows the similar trend for dV_{100-15}. For both type of hcp, the decrease of dV_{15-5} from 100% to ~60% relative humidity and the increase from ~60% to 11% relative humidity can be observed. The dV_{5-1} decreased continuously from 100% to ~60% relative humidity and presented very small amount at low relative humidity both L-hcp and H-hcp.

The alteration of the large capillary pores (dV_{100-15}) associated with the disappearance of small pores (dV_{15-5} and dV_{5-1}) under drying condition due to C-S-H agglomeration. The maximum volume of the large capillary pores at 40% relative humidity induced inevitably the minimum mechanical properties of hcp (i.e. bending strength and Young's modulus) and mortar (i.e. compressive strength) reported by Maruyama [12, 16, 17] and Pihlajavaara [18], respectively.

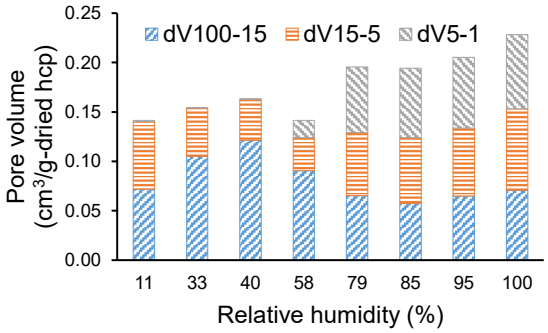

(a) L55

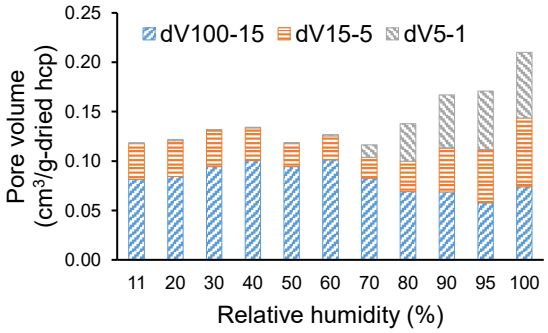

(b) H55

Fig. 7 Nitrogen sorption proportions of the samples

To compare the effect of different cement paste, each range of pore volume was plotted against the relative humidity in Fig. 8. The large capillary pores of L-hcp and H-hcp were similar, but the volumes of small capillary pores and the gel pores shown different proportion. For the small capillary pores and the gel pores, L-hcp shown higher values than H-hcp. Many literatures [19, 20] assumed that the composition and microstructure of C-S-H in alite paste and belite paste are the same. However, in this study, L-hcp showed higher small capillary pores (5-15 nm) and higher gel pores (1-5 nm) than H-hcp due to the difference in the amount of C-S-H and also due to the difference of total porosity.

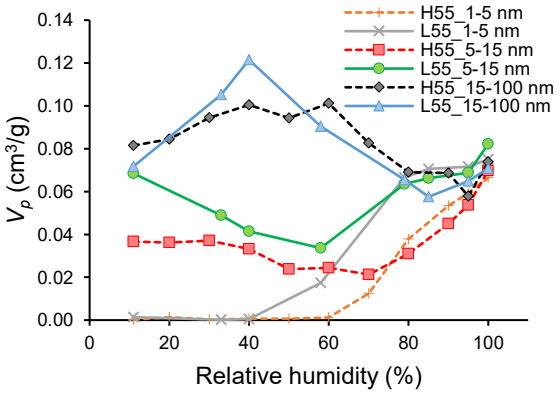

Fig. 8 Comparison between L-hcp and H-hcp on each range of pore volume

4. CONCLUSION

The nitrogen sorption isotherm of two types of hardened cement pastes were measured and simulated by applying GCMC to obtain the pore size distribution. The change of microstructure outside C-S-H under different relative humidity can be presented:

(1) Gel pores in hcp detected by nitrogen sorption at the beginning state of drying (above 58% relative humidity) gradually disappear.
(2) The loss of nitrogen surface area and the reduction of total sorption amount indicate that C-S-H becomes denser from the removal of water. Gel structure gets closer.
(3) The volume of large capillary pores reached a peak at 40% relative humidity both L-hcp and H-hcp.
(4) Comparison between L-hcp and H-hcp, amount of large capillary pores are almost similar, but the small capillary pores and gel pores of L-hcp are higher than H-hcp. Even C_2S in L cement and C_3S in H cement give similar hydration products but those of L-hcp contain more C-S-H and porosity than H-hcp.

ACKNOWLEDGEMENT

These experiments were financial sponsored by Japan Society for the Promotion of Science KAKENHI Grant Number 18H03804.

REFERENCES

[1] Jennings, H. M., Refinements to colloid model of C-S-H in cement: CM-II. Cement and Concrete Research, Vol. 38(3), 2008, pp. 275-289.
[2] Masoero, E., Del Gado, E., Pellenq, R. J. M., Yip, S. and Ulm, F.-J., Nano-scale mechanics of colloidal C–S–H gels. Soft Matter, Vol. 10(3), 2014, pp. 491-499.
[3] Parrott, L. J., Hansen, W. and Berger, R. L., Effect of first drying upon the pore structure of hydrated alite paste. Cement and Concrete Research, Vol. 10(5), 1980, pp. 647-655.
[4] Feldman, R. F. and Sereda, P. J., A model for hydrated Portland cement paste as deduced from sorption-length change and mechanical properties. Matériaux et Construction, Vol. 1(6), 1968, pp. 509-520.
[5] Odler, I., The BET-specific surface area of hydrated Portland cement and related materials. Cement and Concrete Research, Vol. 33(12), 2003, pp. 2049-2056.
[6] Suwanmaneechot, P., Aili, A. and Maruyama, I., Creep behavior of C-S-H under different drying relative humidities: Interpretation of microindentation tests and sorption measurements by multi-scale analysis. Cement and Concrete Research, Vol. 132, 2020, pp. 106036.
[7] Stokes, R. H. and Robinson, R. A., Standard Solutions for Humidity Control at 25° C. Industrial & Engineering Chemistry, Vol. 41(9), 1949, pp. 2013-2013.
[8] Greenspan, L., Humidity fixed points of binary saturated aqueous solutions. Journal of Research of the National Bureau of Standards - A Physics and Chemistry, Vol. 81A(1), 1977, pp. 89-96.
[9] Zhang, J. and Scherer, G. W., Comparison of methods for arresting hydration of cement. Cement and Concrete Research, Vol. 41(10), 2011, pp. 1024-1036.
[10] Brunauer, S., Emmett, P. H. and Teller, E., Adsorption of Gases in Multimolecular Layers. Journal of the American Chemical Society, Vol. 60(2), 1938, pp. 309-319.
[11] Sing, K. S. W., Everett, D. H., Haul, R. A. W., Moscou, L., Pierotti, R. A., Rouquérol, J. and Siemieniewska, T., Reporting physisorption data for gas/solid systems with special reference to the determination of surface area and porosity (Recommendations 1984), in Pure and Applied Chemistry. 1985. pp. 603.
[12] Maruyama, I., Nishioka, Y., Igarashi, G. and Matsui, K., Microstructural and bulk property changes in hardened cement paste during the first drying process. Cement and Concrete Research, Vol. 58, 2014, pp. 20-34.
[13] Lowell, S., Shields, J. E., Thomas, M. A. and Thommes, M., Characterization of porous solids and powders: surface area, pore size and density. 2004: Springer Netherlands.
[14] Zhou, T., Ioannidou, K., Ulm, F.-J., Bazant, M. Z. and Pellenq, R. J. M., Multiscale poromechanics of wet cement paste. Proceedings of the National Academy of Sciences, Vol. 116(22), 2019, pp. 10652.
[15] Maruyama, I., Ohkubo, T., Haji, T. and Kurihara, R., Dynamic microstructural evolution of hardened cement paste during first drying monitored by 1H NMR relaxometry. Cement and Concrete Research, Vol. 122, 2019, pp. 107-117.
[16] Kurihara, R. and Maruyama, I., Effects of heating and drying on the strength and stiffness of high-early-strength Portland cement pastes. Cement and Concrete Composites, Vol. 106, 2020, pp. 103455.
[17] Fujimori, S. and Maruyama, I. Fundamental study on flexural strength of cement paste under different relative humidity. in Summaries of Technical Papers of the Annual Meeting of the Architectural Institute of Japan. 2011.
[18] Pihlajavaara, S. E., A review of some of the main results of a research on the ageing phenomena of concrete: Effect of moisture conditions on strength, shrinkage and creep of mature concrete. Cement and Concrete Research, Vol. 4(5), 1974, pp. 761-771.
[19] Richardson, I. G., The nature of C-S-H in hardened cements. Cement and Concrete Research, Vol. 29(8), 1999, pp. 1131-1147.
[20] Termkhajornkit, P., Vu, Q. H., Barbarulo, R., Daronnat, S. and Chanvillard, G., Dependence of compressive strength on phase assemblage in cement pastes: Beyond gel–space ratio — Experimental evidence and micromechanical modeling. Cement and Concrete Research, Vol. 56, 2014, pp. 1-11.